

Article

Mechanochemical Synthesis of Nickel Mono- and Diselenide: Characterization and Electrical and Optical Properties

Marcela Achimovičová ^{1,*}, Michal Hegedüs ², Vladimír Girman ^{3,4}, Maksym Lisnichuk ^{3,4}, Erika Dutková ¹, Juraj Kurimský ⁵ and Jaroslav Briančin ¹

¹ Institute of Geotechnics, Slovak Academy of Sciences, 04001 Košice, Slovakia

² Synthon s.r.o., 67801 Blansko, Czech Republic

³ Faculty of Science, Pavol Jozef Šafárik University, 04154 Košice, Slovakia

⁴ Institute of Materials Research, Slovak Academy of Sciences, 04001 Košice, Slovakia

⁵ Faculty of Electrical Engineering and Informatics, Technical University, 04200 Košice, Slovakia

* Correspondence: achimovic@saske.sk; Tel.: +421-55-7922607

Abstract: Nickel mono- (NiSe) and diselenide (NiSe₂) were produced from stoichiometric mixtures of powdered Ni and Se precursors by the one-step, undemanding mechanochemical reactions. The process was carried out by high-energy milling for 30 and 120 min in a planetary ball mill. The kinetics of the reactions were documented, and the products were studied in terms of their crystal structure, morphology, electrical, and optical properties. X-ray powder diffraction confirmed that NiSe has hexagonal and NiSe₂ cubic crystal structure with an average crystallite size of 10.5 nm for NiSe and 13.3 nm for NiSe₂. Their physical properties were characterized by the specific surface area measurements and particle size distribution analysis. Transmission electron microscopy showed that the prepared materials contain nanoparticles of irregular shape, which are agglomerated into clusters of about 1–2 μm in diameter. The first original values of electrical conductivity, resistivity, and sheet resistance of nickel selenides synthesized by milling were measured. The obtained bandgap energy values determined using UV–Vis spectroscopy confirmed their potential use in photovoltaics. Photoluminescence spectroscopy revealed weak luminescence activity of the materials. Such synthesis of nickel selenides can easily be carried out on a large scale by milling in an industrial mill, as was verified earlier for copper selenide synthesis.

Keywords: nickel selenide; mechanochemical synthesis; planetary ball mill; nanostructured semiconductor; electrical and optical properties



Citation: Achimovičová, M.; Hegedüs, M.; Girman, V.; Lisnichuk, M.; Dutková, E.; Kurimský, J.; Briančin, J. Mechanochemical Synthesis of Nickel Mono- and Diselenide: Characterization and Electrical and Optical Properties. *Nanomaterials* **2022**, *12*, 2952. <https://doi.org/10.3390/nano12172952>

Academic Editor: Jürgen Eckert

Received: 13 July 2022

Accepted: 23 August 2022

Published: 26 August 2022

Publisher's Note: MDPI stays neutral with regard to jurisdictional claims in published maps and institutional affiliations.



Copyright: © 2022 by the authors. Licensee MDPI, Basel, Switzerland. This article is an open access article distributed under the terms and conditions of the Creative Commons Attribution (CC BY) license (<https://creativecommons.org/licenses/by/4.0/>).

1. Introduction

NiSe and NiSe₂ are members of the VIII-VI binary transition metal chalcogenides group (TMCs). They are p-type semiconductors that scientists are preparing and studying due to their helpful electronic, magnetic, optical, and electrochemical properties applicable in novel smart technologies. NiSe can be used in optical recording materials, optical fibers, sensors, solar cells, laser materials, and conductivity fields [1]. It has also been proposed as a platinum-free catalyst for hydrogen production [2]. In the field of energy storage, NiSe can be a component of Li-ion cells [3]. On the other hand, NiSe₂ presents promising cathode material for future rechargeable Li-ion batteries [4,5] and recently also the anode material for Na-ion batteries [6]. Methods such as solvothermal [3], hydrothermal [7–9], single-source precursor method, thermolysis [1], heating with subsequent milling of the product [10], and polyol technique [10] have so far been used for the synthesis of NiSe. Moreover, different morphologies of NiSe, such as spheres, tubes, nanowires, and flower-shaped structures have been obtained [3,8].

NiSe₂ thin film was prepared by pulsed laser deposition [4], and cubic particles and nanofibers of NiSe₂ were synthesized by one-step solvothermal-reduction [5] and electrospinning process [6]. Zhang and co-workers used a new green acetate-paraffin route

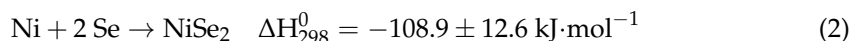
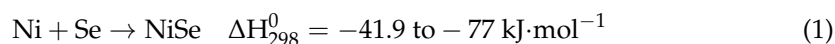
for NiSe₂ synthesis [11]. In 2003, Campos and co-authors reported that the problem with the synthesis of binary nickel selenides alloys which have a substantive difference between the melting point of Ni (1455 °C) and Se (221 °C), could be overcome using the mechanical alloying technique [12]. They successfully obtained nanocrystalline NiSe₂ in the SPEX shaker mill after 10 h of milling.

In terms of a crystal structure, NiSe usually has the hexagonal structure of NiAs. However, the thermodynamically stable rhombohedral structure with a greater anisotropism may also exist. NiSe₂ crystallizes in the cubic-FeS₂ type structure, which has dumbbell-shaped Se₂ units between two Ni atoms [9].

Our several papers and a book chapter deal with the preparation of binary metal selenides and TMCs by the prospective mechanochemical synthesis that can be carried out not only by milling in a laboratory but also in an industrial mill [13–16]. This research describes the hitherto unreported simple mechanosynthesis of nickel mono-NiSe and diselenide NiSe₂ by high-energy milling in a planetary ball mill. Both products were characterized from a structural and morphological point of view; their electrical and optical properties were measured and compared.

2. Materials and Methods

Mechanosynthesis of NiSe and NiSe₂ was performed in the planetary ball mill Pulverisette 6 (Fritsch, Idar-Oberstein, Germany) by the milling of nickel (98.8%, 16 µm, Penta Chemicals Ltd., Prague, Czech Republic) and selenium (99.5%, 74 µm, Aldrich, Darmstadt, Germany) powders according to these reactions:



The negative values of enthalpy change of the reactions (1) and (2) reported in Gmelin's Handbook of Inorganic Chemistry for NiSe_{1.052} and NiSe₂ compounds support their thermodynamic feasibility [17]. The milling conditions were as follows. The calculated amounts of Ni powder, 2.13 g and 1.36 g, and Se powder 2.87 g and 3.64 g with a total mass of 5 g for NiSe and NiSe₂ reactions, were homogenized before milling and put into a tungsten carbide milling chamber with a volume of 250 mL and 50 tungsten carbide balls with a diameter of 10 mm. Subsequently, the milling chamber was filled with an argon atmosphere. The rotation speed was 550 rpm, ball-to-powder ratio 73:1, and milling time from 5 to 120 min.

X-ray powder diffraction patterns (XRPD) of the milled samples were recorded on a Panalytical Empyrean diffractometer working in θ -2 θ Bragg-Brentano geometry using a CuK α _{1,2} X-ray source (0.154439 nm). For the incident beam path, 1/4° fixed divergence slit, 1/2° anti-scatter slit, the mask of 10 mm, and Soller slit (0.02 rad) were used. The diffractometer was equipped with a PIXcel3D detector. The phases were identified using the JCPDS PDF database. The data were analyzed utilizing the Fullprof suite software package [18]. For the Rietveld refinement, the diffraction lines were modeled using the Thomas–Cox–Hastings function. During the refinement, lattice parameters, profile parameters, sample displacement, and background points were refined with atomic parameters kept fixed.

The specific surface area measurements were performed on a Gemini 2360 sorption apparatus (Micromeritics, Norcross, GA, USA) by the low-temperature nitrogen adsorption method.

The particle size analyzer Mastersizer 2000E with a laser diffraction system (Malvern Pananalytical, Malvern, UK), a dry feeder Scirocco 2000M, and the measuring range 0.02–2000 µm were used for the particle size distributions (PSD) measurements.

Scanning electron microscopy (SEM) observations were done with the microscope MIRA3 FE-SEM (TESCAN, Brno, Czech Republic), including an EDX detector (Oxford Instrument, Oxford, UK) for the energy dispersive X-ray analysis (EDX) of the observed samples.

A transmission electron microscopy (TEM) study was performed using a JEOL 2100F UHR microscope operated at 200 kV with a Schottky field emission source. The high-resolution mode was used for taking the images, and the selected area electron diffraction (SAED) was used for the structure identification. Regarding SAED experiments, the microscope was precisely calibrated using MoO₃ crystal. Gold nanoparticles were used for double-checking, as well. The studied samples were dispersed in absolute ethanol and ultrasonicated for 10 min before observation to reduce the agglomeration of the crystals. These sample dispersions were placed on a copper support grid covered with ultra-thin flat carbon film and stored in a vacuum.

A standard four-point probe technique was used to study the electrical properties of the samples [19,20]. The samples in the form of pellets were pressed from 0.41 g of NiSe and NiSe₂ powder products under the pressure of 3 t, without retention time, and at room temperature, in a laboratory hydraulic press (Specac, Fort Washington, PA, USA). The four-point test head (Ossila Ltd., Sheffield, UK) was placed on the measured pellet and fixed to its geometrical center during the measurements with a source-measure unit as reported in our previous work [16]. The probe tips were fixed at the same position and loaded with a constant contact force to obtain reproducible results. The distance between the probe tips was 1.27 mm. The diameter of the circular NiSe and NiSe₂ pellets was 7.06 ± 0.01 mm, and their average room temperature densities of 7.2 and 6.88 g.cm⁻³ were taken from the commonly available literature.

The UV-Vis spectrophotometer Helios Gamma (Thermo Electron Corporation, Warwickshire, UK) was used to measure the optical absorption spectra of the samples. The studied samples were dispersed in absolute ethanol by ultrasonic stirring and poured into the quartz cell.

A photon-counting spectrofluorometer PC1 (ISS, San Antonio, TX, USA) recorded photoluminescence spectra (PL) of the samples at room temperature and with a photoexcitation wavelength of 360 nm. The excitation source was a 300 W xenon lamp, and the widths of the excitation and emission slits were set to 0.5 and 1 mm. The studied samples were dispersed in absolute ethanol by ultrasonic stirring and placed into the quartz cell cuvette for spectral analysis.

3. Results and Discussion

The results of XRPD indicate that the mechanochemical reaction of Ni with Se according to Equation (1), starts with the formation of the NiSe phase (JCPDS 075-0610), which is already present in the system after 5 min of milling (see Figure 1). After the additional 15 min of milling, the product mainly shows the diffraction peaks belonging to the hexagonal NiSe (sederholmite, *P*₆₃/*mmc* space group) with cell parameters $a = 3.66$ Å, $c = 5.33$ Å. Only traces of unreacted elemental nickel metal (JCPDS 004-0850) were detected. Moreover, a weak reflection at 16.5° 2θ might be assigned to the monoclinic wilkmanite Ni₃Se₄ phase (JCPDS 018-0890, *I*₂/*m* space group), which would be in accordance with the observation of unreacted nickel metal. After 30 min of milling, the weight ratio of the NiSe/Ni₃Se₄ phases was determined to be approximately 90/10. The graphical output of the Rietveld refinement in Figure 2 proved that the refined lattice parameters of the NiSe phase are as follows: $a = b = 3.6278(2)$ Å, $c = 5.3318(4)$ Å. The average NiSe crystallite size of 10.5 nm was calculated using the Scherrer formula corrected for instrumental broadening. For the calculation, the integral breadth of (101), (102), (110), and (103) crystallographic planes were used. The provided value is rather informative due to a strong overlap of reflections, high FWHM values, and admixture formation.

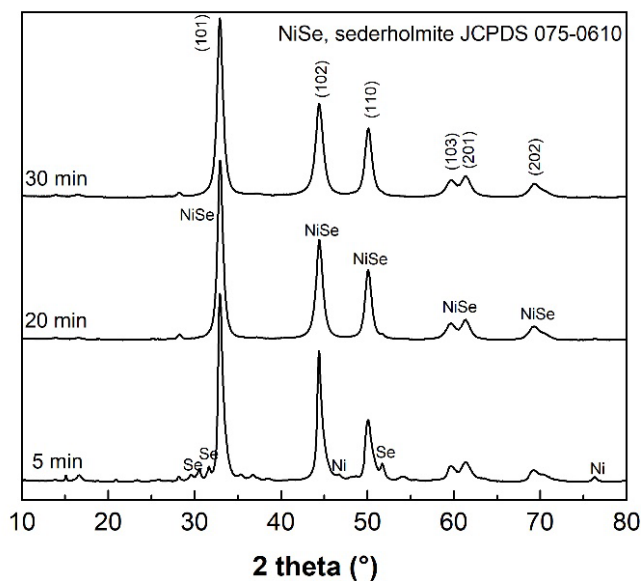


Figure 1. The XRPD patterns of equimolar Ni/Se samples milled for 5, 20, and 30 min.

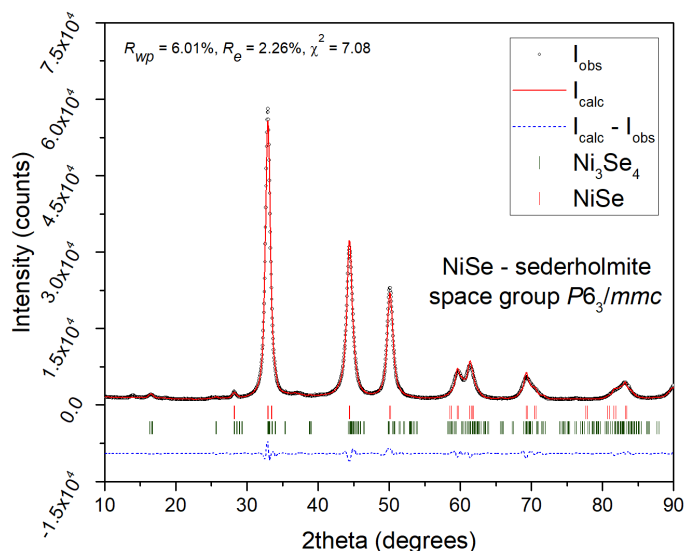


Figure 2. Rietveld refinement graphical output of NiSe—sample milled for 30 min.

The XRPD patterns depicted in Figure 3 confirm the start of the mechanochemical reaction of Ni with 2 Se according to Equation (2) with the formation of the NiSe₂ (JCPDS 011-0552) already after 10 min of milling as well as for NiSe mechanochemical synthesis, following the more negative formation enthalpy compared to the hexagonal NiSe phase. However, the unreacted nickel (JCPDS 004-0850) and selenium (JCPDS 073-0465) peaks clearly predominate. After 90 min of milling, the penroseite NiSe₂ phase with the cubic structure (*Pa*-3 space group) and the cell parameter $a = 5.9604 \text{ \AA}$ as the major product crystallizes. Only traces of unreacted nickel are present in the pattern. The Rietveld refinement of the XRPD data of the 120 min sample (Figure 4) confirmed NiSe₂ phase purity with the refined crystal lattice parameter $a = 5.960 \text{ \AA}$, and the average size of crystallites 13.3 nm.

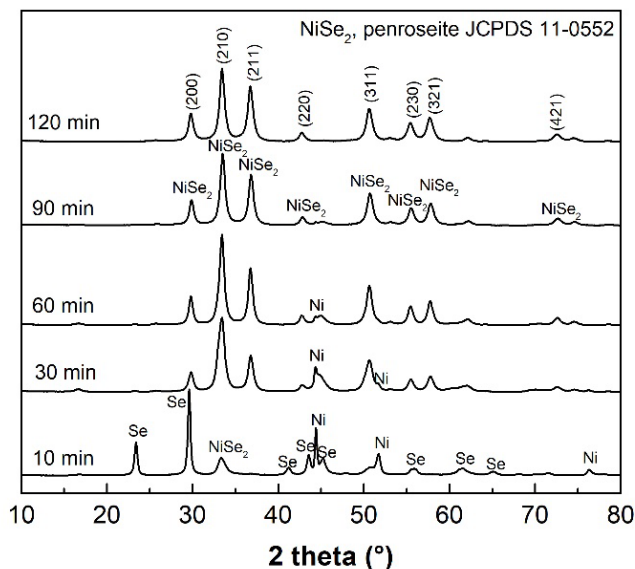


Figure 3. XRPD patterns of Ni/2Se samples milled for 10, 30, 60, 90, and 120 min.

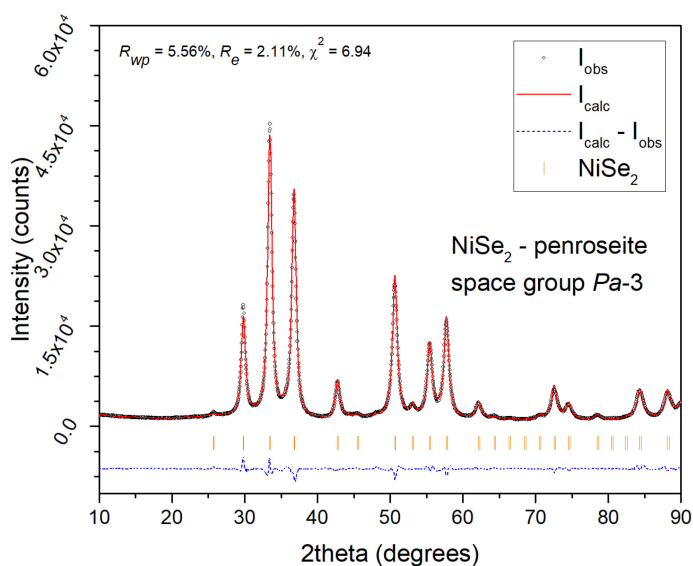


Figure 4. Rietveld refinement graphical outputs of NiSe₂—sample milled for 120 min.

The phase structure, composition, and morphology of mechanochemically synthesized NiSe and NiSe₂ can affect the physical and chemical properties of such uniquely prepared materials.

From the dependences in Figure 5, it follows that the specific surface area, SSA_{BET} of both Ni/Se and Ni/2Se samples increases with the time of milling. The maximum value of $2.39 \text{ m}^2 \cdot \text{g}^{-1}$ for the Ni/Se sample milled for 30 min indicates the completion of the mechanochemical reaction with the formation of the NiSe phase, while the sample Ni/2Se reaches the maximum SSA_{BET} value of $6.73 \text{ m}^2 \cdot \text{g}^{-1}$ after 60 min of milling. Subsequently, the mean particle size of this sample decreases from 2.08 to $1.69 \mu\text{m}$ with increasing milling time, but due to the mutual agglomeration of the particles of the NiSe₂ product, the specific surface area decreases. It is known from the literature that the maximum value of SSA is reached at the end of the mechanochemical reaction for TMCs, but this does not correspond to the case of NiSe₂ [15,21,22].

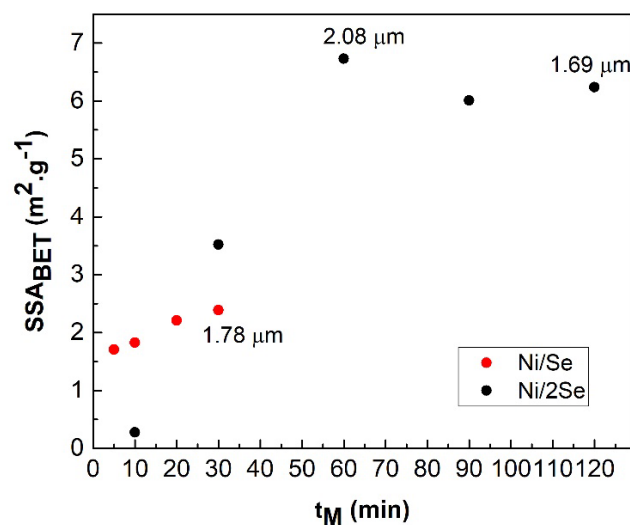


Figure 5. Dependences of specific surface area, SSA_{BET} of Ni/Se and Ni/2Se samples on the time of mechanochemical reaction, t_M with the given numerical values of the mean particle size.

Lower magnification SEM images of the NiSe and NiSe₂ products in Figures 6a and 7a demonstrated the similar agglomerated grains having an irregular shape with inhomogeneous size distribution. The mapping of Ni and Se elements evidenced their homogeneous distribution in both products (Figures 6b and 7b). The quantitative EDX analyses in Figures 6c and 7c confirmed close to the stoichiometric chemical composition of both nickel selenides with atomic ratios of almost 1:1 and 1:2 for NiSe and NiSe₂. A certain deviation in the determination of the elemental composition of the products can probably be caused by their surface which is not entirely flat. The crystallinity and the crystallite size of the products were also examined in more detail by TEM analysis.

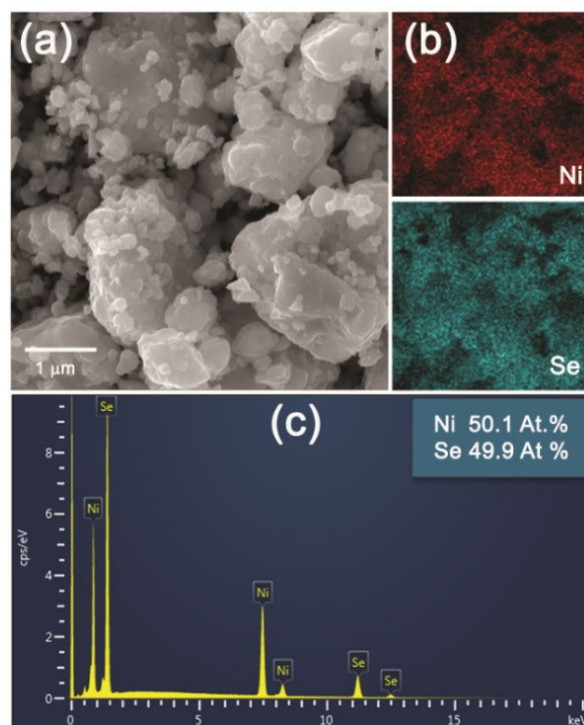


Figure 6. SEM microphotographs of NiSe (a), the element mapping for Ni and Se (b), and EDX analysis (c).

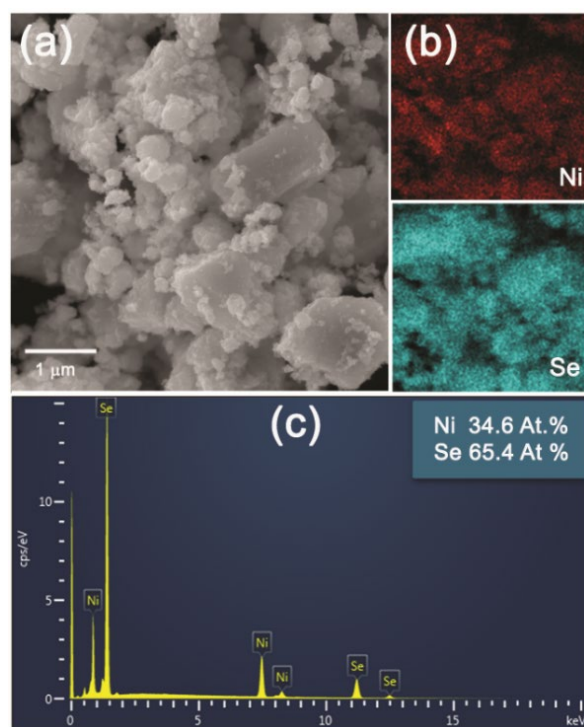


Figure 7. SEM microphotographs of NiSe₂ (a), the element mapping for Ni and Se (b), and EDX analysis (c).

The crystallite size of the NiSe and NiSe₂ samples was calculated based on several images taken in bright field STEM mode to avoid the unwanted diffraction effect. More than 50 crystallites were included in the statistics for each sample. Figure 8b showed the result of the statistics for the sample NiSe in the form of a skewed right histogram. The crystallite size in interval 7–12 nm was observed with the highest frequency. Figure 8a illustrates the agglomerates of crystallites in which some displayed atomic layers. The embedded diffraction pattern confirmed NiSe hexagonal phase with space group $P6_3/mmc$ (194). The calculated average crystallite size of sample NiSe₂ was in the interval of 10–15 nm (Figure 9b), which is a bit more than for sample NiSe. The crystallites of the NiSe₂ sample are visualized in Figure 9a as agglomerated particles. Most of them have distinguishable atomic planes. Analysis of diffraction pattern proved the cubic NiSe₂ phase with space group $Pa-3$ (205). Analyses of selected area electron diffraction are consistent with XRPD results. When comparing the two TEM images Figures 8a and 9a, it should be taken into account that the images were not acquired at the same magnification.

As data on the electrical properties of nickel selenides are very rare in the literature, the electrical conductivity, resistivity, and sheet resistance values of mechanochemically synthesized NiSe and NiSe₂ were investigated and measured. Table 1 shows the resulting values of individual electrical quantities coming from 200 measured values for each product.

Table 1. Electrical quantities of mechanochemically synthesized nickel selenides.

	Product	Mean	Standard Dev	Median
Sheet resistance (mΩ/square)	NiSe	9.34	6.94	7.00
	NiSe ₂	6.26	0.87	6.32
Resistivity (μΩ m)	NiSe	19.98	14.85	14.97
	NiSe ₂	14.43	2.01	14.57
Conductivity (kS/m)	NiSe	68.80	32.82	66.78
	NiSe ₂	70.71	10.42	68.64

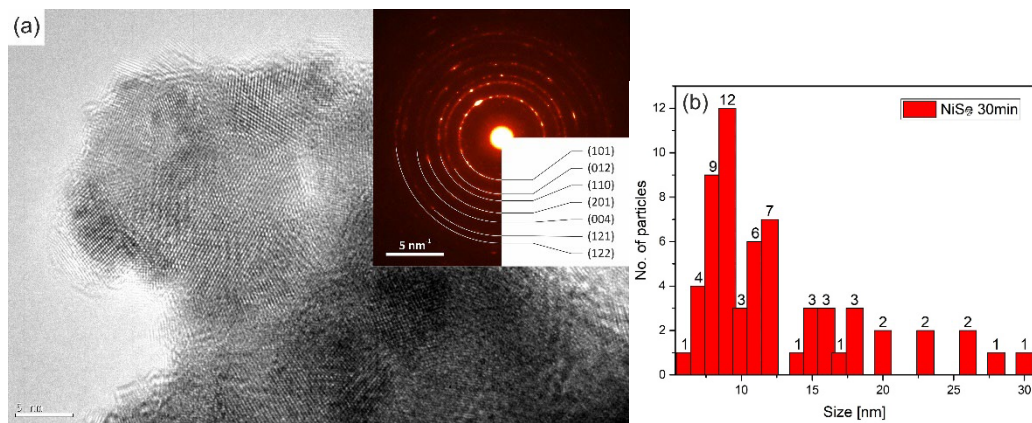


Figure 8. High-resolution TEM micrograph of NiSe agglomerated crystals—magnification 400 kx (a) with inset SAED pattern, particle size distribution analysis from TEM observation (b).

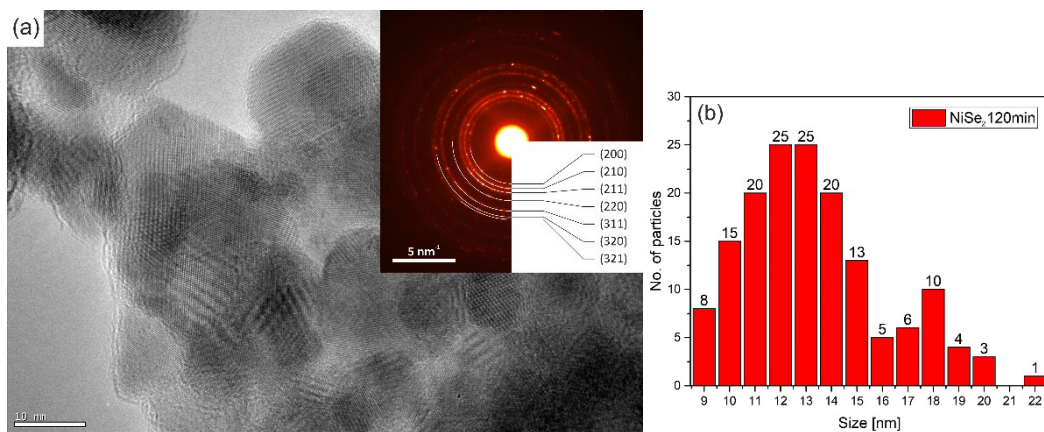


Figure 9. High-resolution TEM micrograph of NiSe₂ agglomerated crystals—magnification 300 kx (a) with inset SAED pattern, particle size distribution analysis from TEM observation (b).

The conductivity of NiSe₂ is slightly higher than that of NiSe, which is related to the larger crystallite size of NiSe₂ (10–15 nm). This crystallite and/or grain size effect is even more evident at the resistivity value, which is significantly lower for NiSe₂ than for NiSe (7–12 nm). The electrical resistivity values at room temperature are of the same order as the values reported for nickel selenide prepared by chemical deposition [23], and the solid-state reaction method [24]. The descriptive statistics were performed from the values measured on 20 samples. High standard deviations for the NiSe sample indicate a problem with reproducing the electrical properties of the sample prepared by mechanochemical synthesis. We note that separate statistics for individual samples provide the expected standard deviation, however with significant variation in their mean values.

Nickel selenides are classified as p-type semiconductors, and their bandgap energy value is 620 nm (2.0 eV). According to the literature, the bandgaps of NiSe and NiSe₂ are narrower than that of nickel oxide (3.6–4.0 eV) and wider than bulk nickel sulphide (0.4 eV). Therefore, they also become potential candidates for solar cells [10]. Figure 10 shows the measured UV–Vis optical absorption spectra of both mechanochemically synthesized nickel mono- and diselenides. Both nickel selenides absorbed UV–Vis radiation in the entire range from 200 to 1000 nm, which fits well when using the solar spectrum. The slightly smaller particles and nanocrystallites of NiSe likely caused the weak excitonic peak at 218 nm (5.65 eV).

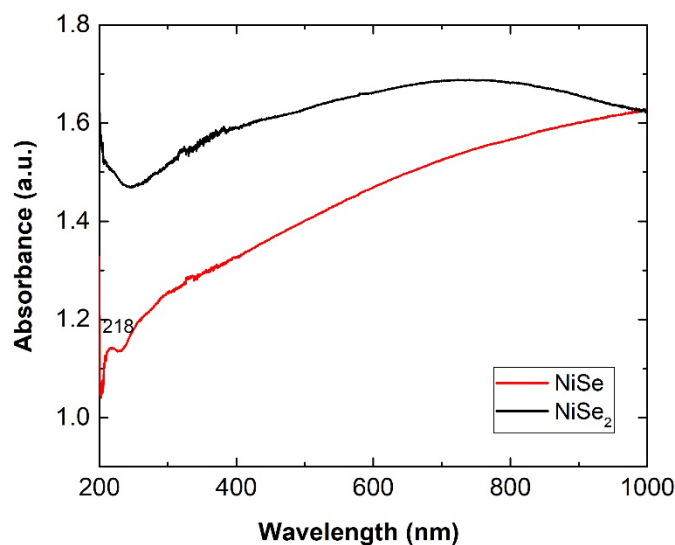


Figure 10. Mono- and diselenide optical absorption spectra.

For NiSe₂, no excitonic peak was observed in the spectrum. The linear part of the Tauc plots in Figure 11 indicates that the NiSe and NiSe₂ semiconductors involve a direct optical transition. The bandgaps 1.35 eV for NiSe and 1.9 eV for NiSe₂ were determined by extrapolating the linear regions of the plots to $(\alpha h\nu)^2 = 0$. The bandgap value of NiSe is red-shifted compared to the value of bulk NiSe as well as the value of 1.61 eV for NiSe thin films prepared by chemical deposition and reported by Hankare and co-authors [23]. The determined value of NiSe₂ bandgap energy more or less corresponds to the bandgap of bulk nickel selenide (2.0 eV).

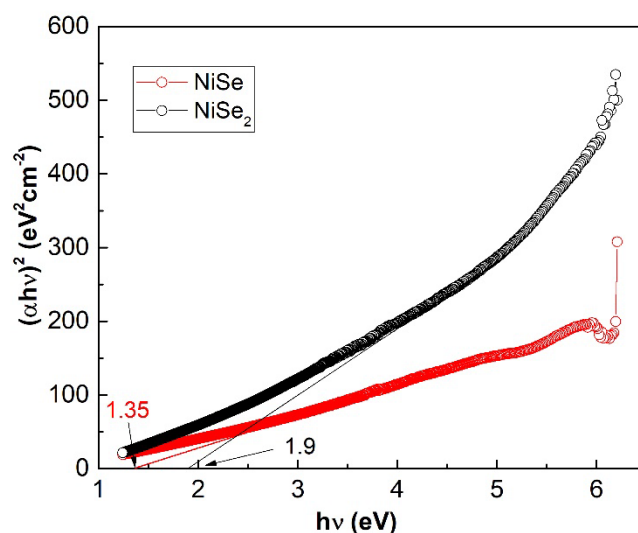


Figure 11. Tauc plots of mono- and diselenide with the obtained bandgaps 1.35 and 1.9 eV.

The room temperature PL emission spectra of nickel selenides are shown in Figure 12. Light with a wavelength of 360 nm and corresponding to a photon energy of 3.42 eV was used for irradiation—photoexcitation of the samples. This photon energy is absorbed to excite the transition of electrons from the valence band to the conduction band.

Regarding the peak position, the situation is similar in both samples. The samples have a broad violet emission around 410 nm (3 eV). However, the emission peak of the NiSe₂ sample has a slightly lower luminescence intensity than NiSe one. Since the emission of PL radiation is mainly due to the recombination of photo-excited electrons and holes,

the lower PL intensity could indicate a lower rate of electron/holes recombination in NiSe₂. Our results are in accordance with previously published papers [1,8,25]. The emission peak situated at 410 nm may be attributed to the defects. These defects occurring in the nanocrystals are generated as a result of high-energy milling. Nevertheless, both samples exhibit only weak photoluminescence.

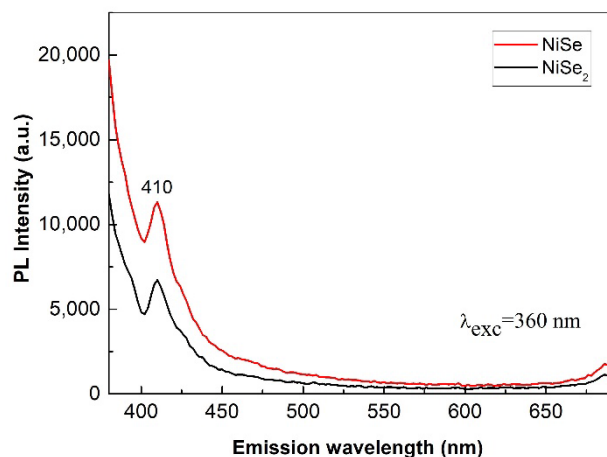


Figure 12. Mono- and diselenide PL emission spectra at an excitation wavelength of 360 nm.

Table 2 summarizes literature data on NiSe and NiSe₂ synthesized by various techniques, including mechanochemical synthesis. By comparing the energy and time requirements of individual preparation methods, mechanosynthesis in the planetary mill is a fast, one step, and takes place at ambient temperature. In addition, it does not require solvents, additional reagents, or subsequent operations such as washing and drying the product. The crystallite sizes of NiSe and NiSe₂ prepared by our procedure reach low values, which could enable their possible applications listed in Table 2 for nickel selenides synthesized by other conventional methods. However, verification and further research are needed.

Table 2. Comparison of the nickel selenides characteristics synthesized by various techniques.

	Method	Temperature/Time	Size	Morphology	Possible Application	Ref.
NiSe	Thermolysis	160 °C/1 h	~150 nm	Star-shaped	Solar technology	[1]
	Solvothermal	180 °C/12 h	10–20 nm ≤ 500 nm	Nanofibers	Electrocatalyst for H ₂ production	[2]
	Solvothermal	140 °C/24 h	50 μm	Microtubes	Cathode material for LIBs	[3]
	Polyol	220 °C/3 h	7–9 nm	Nanoparticles	Catalyst: reduction of org. molecules	[10]
	Heating and subseq. milling	960 °C/10 h	7–11 nm	Crystallites	Catalyst: reduction of toxic chemicals	[10]
	Milling in planetary mill	-/30 min	10.5 nm	Crystallites	Unexamined	[this work]
NiSe ₂	Pulsed laser deposition		50 nm	Thin film	Cathode material for LIBs	[4]
	Solvothermal reduction	180–280 °C/1 h	30–50 nm	Cubes	Unexamined	[5]
	Electrospinning and subseq. selenization	450 °C/3 h 300 °C/10 h	27 nm	Nanofibers	Anode material for SIBs	[6]
	Hydrothermal	140 °C/20 h	3–4 μm	Octahedral crystals	Unexamined	[9]
	Milling in Spex mill	-/30 h	25 nm	Crystallites	Unexamined	[12]
	Milling in planetary mill	-/2 h	13.3 nm	Crystallites	Unexamined	[this work]

4. Conclusions

Simple, one-step, solvent-free, ecological, relatively economically undemanding, and possible large-scale mechanochemical synthesis of mono- (NiSe) and diselenide (NiSe₂) nanostructured semiconductors nickel was carried out. XRPD proved that NiSe and NiSe₂ products with average crystallite sizes of 10.5 and 13.3 nm were synthesized by milling for 30 and 120 min in the planetary ball mill. Rietveld analysis confirmed the hexagonal structure of NiSe (JCPDS 075-0610, space group *P6₃/mmc*) and the cubic structure of NiSe₂ (JCPDS 011-0552, space group *Pa-3*). Both products contain irregularly shaped nanoparticles that form approximately 1–2 μm agglomerates, as revealed by SEM observations. Qualitative EDX analysis revealed that the atomic ratio of Ni:Se is almost 1:1 and 1:2 for NiSe and NiSe₂. The results of TEM analyses, SAED patterns indexing, and particle size analyses were in good agreement with the XRPD results. Regarding electrical properties measured for the first time for mechanochemically synthesized nickel selenides, the conductivity of NiSe₂ was slightly higher, and resistivity was lower than that of NiSe, which is related to the larger crystallite size of NiSe₂. The calculated energy bandgaps of 1.35 and 1.9 eV for NiSe and NiSe₂ are in the range suitable for photovoltaics. Their PL spectra showed only a weak emission at 410 nm, which may be attributed to the defects generated by high-energy milling.

Author Contributions: Conceptualization, M.A. and M.H.; methodology, M.H., J.K., V.G., M.L., E.D. and J.B.; investigation, M.A.; writing—original draft preparation, M.A.; writing—review and editing, M.H., V.G. and E.D. All authors have read and agreed to the published version of the manuscript.

Funding: This research was realized within the frame of the project “Research Centre of Advanced Materials and Technologies for Recent and Future Applications PROMATECH”, ITMS 26220220186, supported by the Operational Program “Research and Development” financed through European Regional Development Fund, Slovak Research and Development Agency under the contract No. APVV-18-0357 and APVV-18-0160 and by the Slovak Grant Agency VEGA (projects 2/0103/20, 02/0011/20).

Institutional Review Board Statement: Not applicable.

Informed Consent Statement: Not applicable.

Data Availability Statement: The data presented in this study are available on request from the corresponding author.

Acknowledgments: The authors would like to thank R. Bureš for performing the PSD analyses of the samples and Lev P. Roda for final editing.

Conflicts of Interest: The authors declare no conflict of interest. The funders had no role in the design of the study; in the collection, analyses, or interpretation of data; in the writing of the manuscript, or in the decision to publish the results.

References

1. Moloto, N.; Moloto, M.; Coville, N.; Ray, S. Optical and structural characterization of nickel selenide nanoparticles synthesized by simple methods. *J. Cryst. Growth* **2009**, *311*, 3924–3932. [[CrossRef](#)]
2. Gao, M.; Lin, Z.; Zhuang, T.; Jiang, J.; Xu, Y.; Zheng, Y.; Yu, S. Mixed-solution synthesis of sea urchin-like NiSe nanofiber assemblies as economical Pt-free catalysts for electrochemical H₂ production. *J. Mater. Chem.* **2012**, *22*, 13662–13668. [[CrossRef](#)]
3. Mi, L.; Sun, H.; Ding, Q.; Chen, W.; Liu, C.; Hou, H.; Zheng, Z.; Shen, C. 3D hierarchically patterned tubular NiSe with nano-/microstructures for Li-ion battery design. *Dalton T.* **2012**, *41*, 12595–12600. [[CrossRef](#)]
4. Xue, M.; Fu, Z. Lithium electrochemistry of NiSe₂: A new kind of storage energy material. *Electrochem. Commun.* **2006**, *8*, 1855–1862. [[CrossRef](#)]
5. Yuan, B.; Luan, W.; Tu, S. One-step solvothermal synthesis of nickel selenide series: Composition and morphology control. *Cryst. Eng. Comm* **2012**, *14*, 2145–2151. [[CrossRef](#)]
6. Cho, J.; Lee, S.; Kang, Y. First introduction of NiSe₂ to anode material for sodium-ion batteries: A hybrid of graphene-wrapped NiSe₂/C porous nanofiber. *Sci. Rep.* **2016**, *6*, 23338. [[CrossRef](#)]
7. Sobhani, A.; Davar, F.; Salavati-Niasari, M. Synthesis and characterization of hexagonal nano-sized nickel selenide by simple hydrothermal method assisted by CTAB. *Appl. Surf. Sci.* **2011**, *257*, 7982–7987. [[CrossRef](#)]
8. Sobhani, A.; Salavati-Niasari, M.; Davar, F. Shape control of nickel selenides synthesized by a simple hydrothermal reduction process. *Polyhedron* **2012**, *31*, 210–216. [[CrossRef](#)]

9. Zhuang, Z.; Peng, Q.; Zhuang, J.; Wang, X.; Li, Y. Controlled hydrothermal synthesis and structural characterization of a nickel selenide series. *Chem. Eur. J.* **2006**, *12*, 211–217. [[CrossRef](#)]
10. Subbarao, U.; Marakatti, V.; Amshumali, M.; Loukya, B.; Singh, D.; Datta, R.; Peter, S. Size and morphology controlled NiSe nanoparticles as efficient catalyst for the reduction reactions. *J. Solid State Chem.* **2016**, *244*, 84–92. [[CrossRef](#)]
11. Zhang, A.; Ma, Q.; Lu, M.; Zhou, G.; Li, C.; Wang, Z. Nanocrystalline metal chalcogenides obtained open to air: Synthesis, morphology, mechanism, and optical properties. *J. Phys. Chem. C* **2009**, *113*, 15492–15496. [[CrossRef](#)]
12. Campos, C.; de Lima, J.; Grandi, T.; Machado, K.; Pizani, P.; Hinrichs, R. Nucleation and growth of nanocrystalline pyrite nickel diselenide by mechanical alloying. *Solid State Commun.* **2003**, *128*, 229–234. [[CrossRef](#)]
13. Achimovičová, M.; Baláž, P. Nanocrystalline Metal Selenides: Mechanochemical Synthesis and Utilizable Properties. In *Milling Fundamentals, Processes and Technologies*; Ramirez, M., Ed.; NOVA Science Publishers Inc.: New York, NY, USA, 2015; pp. 71–122.
14. Achimovičová, M.; Daneu, N.; Dutková, E.; Zorkovská, A. Mechanochemically synthesized cobalt monoselenide: Structural characterization and optical properties. *Appl. Phys. A Mater.* **2017**, *123*, 154. [[CrossRef](#)]
15. Achimovičová, M.; Daneu, N.; Tóthová, E.; Mazaj, M.; Dutková, E. Combined mechanochemical/thermal annealing approach for the synthesis of Co₉Se₈ with potential optical properties. *Appl. Phys. A Mater.* **2019**, *125*, 8. [[CrossRef](#)]
16. Achimovičová, M.; Baláž, M.; Girman, V.; Kurimský, J.; Briančin, J.; Dutková, E.; Gáborová, K. Comparative study of nanostructured CuSe semiconductor synthesized in a planetary and vibratory mill. *Nanomaterials* **2020**, *10*, 2038. [[CrossRef](#)]
17. Pietsch, H.E.E. (Ed.) *Gmelin's Handbook of Inorganic Chemistry*, 8th ed.; Springer: Berlin/Heidelberg, Germany, 1955; p. 710.
18. Rodríguez-Carvajal, J. Recent developments of the program FullProf. *Comm. Powder Diffraction IUCr Newsl.* **2001**, *26*, 12–19.
19. Topsoe, H. Geometric correction factors in four point resistivity measurement. *Semiconduct. Division* **1968**, *63*, 472.
20. Kumar, V.; Kelekanjeri, G.; Gerhardt, R. A closed-form solution for the computation of geometric correction factors for four-point resistivity measurements on cylindrical specimens. *Meas. Sci. Technol.* **2008**, *19*, 025701. [[CrossRef](#)]
21. Achimovičová, M.; Daneu, N.; Rečnik, A.; Ďurišin, J.; Baláž, P.; Fabián, M.; Kováč, J.; Šatka, A. Characterization of mechanochemically synthesized lead selenide. *Chem. Pap.* **2009**, *63*, 562–567. [[CrossRef](#)]
22. Achimovičová, M.; Gotor, F.; Real, C.; Daneu, N. Mechanochemical synthesis and characterization of nanocrystalline BiSe, Bi₂Se₃ semiconductors. *J. Mater. Sci. Mater. El.* **2012**, *23*, 1844–1850. [[CrossRef](#)]
23. Hankare, P.; Jadhav, B.; Garadkar, K.; Chate, P.; Mulla, I.; Delekar, S. Synthesis and characterization of nickel selenide thin films deposited by chemical method. *J. Alloy. Compd.* **2010**, *490*, 228–231. [[CrossRef](#)]
24. Chin, P.Y. *Structural, Electrical, Optical and Thermal Properties of Nickel Selenide*; Universiti Putra Malaysia: Serdang, Malaysia, 2015.
25. Ling, L.; Zhu, L.; Zhang, Q.; Wang, C.; Chen, S. Interface-spawned NiSe quantum dots: Preparation, photoluminescence properties and applications. *J. Mater. Chem. C* **2015**, *3*, 473–478. [[CrossRef](#)]